

1 **Integrating laboratory and field data to quantify the**
2 **immersion freezing ice nucleation activity of mineral dust**
3 **particles**

4
5 **Paul J. DeMott¹, Anthony J. Prenni^{1,*}, Gavin R. McMeeking², Ryan C. Sullivan³,**
6 **Markus D. Petters⁴, Yutaka Tobo^{1,#}, Monika Niemand⁵, Ottmar Möhler⁵,**
7 **Jefferson R. Snider⁶, Zhien Wang⁶, and Sonia M. Kreidenweis¹**

8 [1]{ Department of Atmospheric Science, Colorado State University, Fort Collins, CO 80523-
9 1371, USA }

10 [2]{ Droplet Measurement Technologies, Boulder, CO, USA }

11 [3]{ Center for Atmospheric Particle Studies, Carnegie Mellon University, Pittsburgh, PA,
12 USA }

13 [4]{ Department of Marine and Atmospheric Sciences, North Carolina State University,
14 Raleigh, NC, USA }

15 [5]{ Institute for Meteorology and Climate Research – Atmospheric Aerosol Research,
16 Karlsruhe Institute of Technology, Karlsruhe, Germany }

17 [6]{ Department of Atmospheric Sciences, University of Wyoming, Laramie, WY, USA }

18 [*]{Now at: Air Resources Division, National Park Service, Denver, CO}

19 [#]{Now at: National Institute of Polar Research, Tachikawa, Tokyo 190-8518, Japan}

20 Correspondence to: P. J. DeMott (Paul.DeMott@Colostate.edu)

21

22 **Abstract**

23 Data from both laboratory studies and atmospheric measurements are used to develop an
24 empirical parameterization for the immersion freezing activity of natural mineral dust
25 particles. Measurements made with the Colorado State University (CSU) continuous flow
26 diffusion chamber (CFDC) when processing mineral dust aerosols at a nominal 105% relative
27 humidity with respect to water (RH_w) are taken as a measure of the immersion freezing

28 nucleation activity of particles. Ice active frozen fractions versus temperature for dusts
29 representative of Saharan and Asian desert sources were consistent with similar
30 measurements in atmospheric dust plumes for a limited set of comparisons available. The
31 parameterization developed follows the form of one suggested previously for atmospheric
32 particles of non-specific composition in quantifying ice nucleating particle concentrations as
33 functions of temperature and the total number concentration of particles larger than 0.5 μm
34 diameter. Such an approach does not explicitly account for surface area and time
35 dependencies for ice nucleation, but sufficiently encapsulates the activation properties for
36 potential use in regional and global modeling simulations, and possible application in
37 developing remote sensing retrievals for ice nucleating particles. A calibration factor is
38 introduced to account for the apparent underestimate (by approximately 3, on average) of the
39 immersion freezing fraction of mineral dust particles for CSU CFDC data processed at an
40 RH_w of 105% versus maximum fractions active at higher RH_w . Instrumental factors that affect
41 activation behaviour versus RH_w in CFDC instruments remain to be fully explored in future
42 studies. Nevertheless, the use of this correction factor is supported by comparison to ice
43 activation data obtained for the same aerosols from Aerosol Interactions and Dynamics of the
44 Atmosphere (AIDA) expansion chamber cloud parcel experiments. Further comparison of the
45 new parameterization, including calibration correction, to predictions of the immersion
46 freezing surface active site density parameterization for mineral dust particles, developed
47 separately from AIDA experimental data alone, shows excellent agreement for data collected
48 in a descent through a Saharan aerosol layer. These studies support the utility of laboratory
49 measurements to obtain atmospherically-relevant data on the ice nucleation properties of dust
50 and other particle types, and suggest the suitability of considering all mineral dust as a single
51 type of ice nucleating particle as a useful first order approximation in numerical modeling
52 investigations.

53

54

55

56

57

58

60 **1 Introduction**

61 Ice nucleation by atmospheric aerosols impacts the microphysical composition, radiative
62 properties and precipitation processes in clouds colder than 0°C. Since the processes
63 responsible for ice nucleation are not fully understood at the molecular level, and it has yet to
64 be demonstrated that the full variety of surface property influences on ice nucleation by the
65 many types of aerosols present in the atmosphere can be described by phenomenological
66 models, there is need to simplify description of ice nucleation as understood through
67 measurements. Even with an improved understanding of ice nucleation from a fundamental
68 standpoint, there will remain a need for simplified schemes to describe ice nucleation in
69 computationally intensive numerical models and for developing links between aerosol optical
70 properties and ice nucleating particle concentration profiles using remote sensing
71 measurements (Seifert et al. 2011).

72 Complete description of ice nucleation for ice nucleating particles (INPs), INP and INPs
73 being terms we will adopt in this paper following Vali (2014), requires consideration of all
74 relevant heterogeneous ice nucleation mechanisms. As defined by Vali (1985), these
75 mechanisms involve either deposition of ice from the vapour phase (deposition nucleation) or
76 freezing of a particle liquid phase in the bulk of cloud droplets (immersion freezing), during
77 action as a CCN (condensation freezing), or after collision of a particle with the surface of a
78 liquid droplet (contact freezing). The relative importance of different ice nucleation
79 mechanisms will be affected by INP mixing state, and also the cloud formation conditions and
80 the thermodynamic path followed by particles entering clouds. Thus, for example, particles
81 reaching cold cloud regions through the base of warm-based cumulus clouds may have a high
82 likelihood of being within supercooled droplets at the point of freezing, whereas those
83 entering the base of an altocumulus cloud at below -20°C may be available to act via
84 deposition and condensation or immersion freezing. We consider that immersion freezing
85 may be the most critical mechanism for quantifying ice nucleation in moderately supercooled
86 clouds because most INPs reaching supercooled cloud conditions arrive having spent
87 substantial time in clouds, and potentially serving as CCN by virtue of their sizes and/or
88 compositions. Murray et al. (2012) summarize additional observational support for the
89 relative major importance of immersion freezing nucleation.

90 Data for developing simplified descriptions, or parameterizations, of INP concentrations may
91 come exclusively from laboratory data (e.g., Niemand et al., 2012), exclusively from field
92 data (Tobo et al., 2013), or may combine laboratory and field data to test or constrain
93 parameterization frameworks (Phillips et al., 2008, 2013; Niemand et al., 2012). Situations
94 can occur for which a certain particle type dominates INPs during field measurements, and
95 this offers the opportunity to investigate the consistency of laboratory and field measurements
96 for the particular type of INP, and to thereby develop more representative parameterizations.
97 This study emphasizes quantifying immersion freezing nucleation using laboratory and field
98 measurements made with the Colorado State University (CSU) continuous flow diffusion
99 chamber (CFDC) ice nucleation instrument. This instrument, described in detail by Rogers
100 (1988) and Rogers et al. (2001), is designed to focus a flowing stream of particles in a narrow
101 lamina within the water vapor and temperature gradient fields created between two cylindrical
102 ice surfaces held at different temperatures in order to expose the particles to well-defined
103 temperature and relative humidity conditions that promote ice nucleation. We will herein
104 equate freezing nucleation occurring when operating the CFDC in the substantially
105 supersaturated regime with respect to liquid water to immersion freezing since processing
106 particles in this manner favors rapid formation of droplets prior to subsequent freezing (see
107 next section). Recent studies for which CFDC measurements were made together with
108 instruments or methods that mimic the immersion freezing process more explicitly support
109 this assumption (Sullivan et al., 2010a; Niedermeier et al., 2011a; Garcia et al., 2012; Wex et
110 al., 2014).

111 DeMott et al. (2010) applied similar considerations in developing a simplified
112 parameterization of INP number concentrations of all compositional types intended for global
113 model use on the basis of field data collected in multiple campaigns using the CSU CFDC
114 instrument. Interpreting CFDC data in a deterministic manner (see Appendix A), DeMott et
115 al. (2010), hereafter D10, demonstrated that incorporating dependence of INP number
116 concentrations on aerosol number concentrations larger than 0.5 μm greatly improved
117 predicted INP compared to including temperature dependence alone. It was acknowledged
118 that additional aerosol compositional dependencies might explain some of the variance
119 remaining in observed INP number concentrations versus values predicted by the D10
120 parameterization. This contention is supported by the fact that Tobo et al. (2013) observed
121 systematic errors of predicted (D10) versus measured INP number concentration at a single
122 forest site, which appeared to have been dominated by biological INPs. In the present study,

123 we seek to follow the approach of D10 and Tobo et al. (2013), but apply it exclusively to data
124 on mineral dust INPs collected in the laboratory and in field measurements where mineral
125 dust particles dominated in the layers where aircraft CFDC observations of INP number
126 concentration were made. In this way, comparison can be made to a method that utilized only
127 laboratory data from testing of varied mineral dust particles in the Aerosol Interactions and
128 Dynamics of the Atmosphere (AIDA) chamber for development of an ice nucleation
129 parameterization (Niemand et al., 2012).

130

131 **2 Methods**

132 All laboratory data used in this paper were collected during sampling at the AIDA chamber in
133 the ICIS-2007 (International workshop on Comparing Ice nucleation measuring Systems -
134 2007) campaign (DeMott et al., 2011) and the ACI03 (3rd Aerosol-Cloud Interaction)
135 campaign, held in 2009. In these campaigns, multiple instruments sampled particles from a 4
136 m³ aerosol chamber, and sometimes from the larger (84 m³) AIDA chamber prior to cloud-
137 forming expansions. Field study data are used from the Pacific Dust experiment (Stith et al.,
138 2009) flown over the Pacific Ocean basin on the NSF/NCAR G-V aircraft in 2007, and the
139 2011 Ice in Clouds – Tropical clouds study (ICE-T) flown on the NSF/NCAR C-130 aircraft
140 from St. Croix, U.S. Virgin Islands (Heymsfield and Willis, 2014). The former study focused
141 on Asian dust transports in the mid- to upper troposphere, while the latter study emphasized
142 the influence of the Saharan Aerosol Layer on ice formation in tropical cumuli. The use of
143 these data in this study is described in this section.

144 **2.1 Use and interpretation of CFDC data**

145 As done in D10, INP number concentrations active during the CFDC residence time for
146 periods of stable conditions of the processing temperature in degrees Kelvin (T_k), relative
147 humidity with respect to water (RH_w), and pressure were tabulated as a function of aerosol
148 particle concentrations for particles with diameters $>0.5 \mu\text{m}$. Also as in D10, CFDC data were
149 considered as deterministic outcomes rather than reflecting time-dependent nucleation rates.
150 A brief discussion of this assumption, its possible validity and implications are given in
151 Appendix A. Data were stratified at 5°C temperature intervals, with a 1°C difference allowed
152 about the target value. Finally, a reference condition was placed on the processing RH_w
153 deemed representative of immersion freezing nucleation. To explain the reason for and choice

154 of a reference value, it is necessary to briefly review the CFDC principles of operation
155 described in detail in other publications (e.g., Rogers, 1988; Rogers et al., 2001).

156 Aerosol enters the CFDC starting from ambient temperature conditions, but reduced to
157 temperatures already below 273 K during entry into the insulated CFDC inlet manifold and
158 with relative humidity lowered already by passage through diffusion dryers (DeMott et al.,
159 2009). The aerosol lamina, representing typically 15% of the total flow, passes downward
160 between sheath flows in the vertically-oriented, cylindrical CFDC. In Fig. 1, calculations
161 made based on the model of Rogers (1988) and focused at the central position of the aerosol
162 lamina show how the sample rapidly cools and adjusts $SS_w (= RH_w - 100\%)$ over 1 to 3 s in
163 the upper part of the vertical chamber. The nearly steady-state central lamina temperature,
164 -30°C in Fig. 1, is determined by the warm (outer) and cold (inner) wall ice surface
165 temperatures. Cooling of a few tenths of a degree continues as the SS_w rises from subsaturated
166 conditions to 5% for the case shown in Fig. 1. Depending on temperature, particle phase state
167 and CCN activation properties, deposition nucleation may be possible or the particle will
168 otherwise be immersed in a cloud droplet, favoring ice activation by condensation and
169 immersion freezing, which we will assume not to distinguish here. The CSU CFDC design
170 uses evaporation of liquid water droplets followed by optical particle sizing to differentiate
171 activated INPs, grown to ice crystal sizes, from other aerosols. Evaporation is forced by the
172 setting of equal (cold) ice wall temperatures in the lower $\sim 1/3$ of the CSU CFDC (Rogers et
173 al., 2001; DeMott et al., 2010), or after about 4.7s for the conditions in Fig. 1. Ice crystals
174 survive the evaporation region, typically at sizes much larger than $3\ \mu\text{m}$ (not shown), used as
175 the “cut-point” size separating ice versus liquid in this study. Unfrozen liquid water droplets
176 are reduced in size, at least until a certain steady state supersaturation is exceeded in the upper
177 growth section of the CFDC, whereupon droplets grow too large to shrink below the ice cut-
178 point size in the time spent in the evaporation region. This high RH_w limit has been referred to
179 as the “droplet breakthrough” RH_w (Stetzer et al., 2008). For the typical operational flow rate
180 conditions used for the CSU CFDC, this is predicted to occur when RH_w approaches 109% if
181 a condensation coefficient of 1 is assumed for water growth and evaporation calculations
182 when starting from the submicron (dry) sizes of particles typically generated for laboratory
183 studies (Fig. 1). This will be a limitation specific to the geometry and flow rate of all
184 continuous flow ice thermal diffusion chambers unless an explicit water/ice phase
185 discrimination method is used for counting INPs.

186 Figure 2 confirms the reasonableness of the calculated upper RH_w limitation for the CSU
187 CFDC (Fig. 1), showing droplet breakthrough occurring at 108.5% RH_w while sampling
188 mineral dust particles with a size mode at about 0.2 μm and the size parameters stated in the
189 caption of Fig. 2. The calculations in Fig. 1 are made for monodisperse 0.3 micron particles.
190 Droplet breakthrough is indicated in Fig. 2 by the point at which the apparent INP active
191 fraction ($= n_{INP}/n_a$ where n_a is total particle concentration measured with a condensation
192 particle counter) rises sharply with further RH_w increase. RH_w values for this upper limit
193 exceeding 110% have been observed in some other laboratory studies (Petters et al., 2009;
194 DeMott et al., 2011), and this likely relates to modest variations in the total length of exposure
195 to the ice-coated growth region of the CFDC due to manually controlling the water volume
196 pumped into the CFDC chamber during wall icing cycles. In practice, when sampling
197 atmospheric particle distributions, we have observed droplet breakthrough to occur at between
198 106.5 to 108.5% RH_w for the CSU CFDC. This is in part due to sampling particles with sizes
199 up to the 50% cut-point limit of 1.5 to 2.4 micron inlet impactors used operationally in
200 different studies to assure that larger particles are not falsely counted as ice crystals. Droplet
201 breakthrough RH_w also depends on processing temperature, as discussed by Richardson
202 (2009).

203 Due to this upper RH_w limitation for processing, a reference or normalizing RH_w condition for
204 assembling common CFDC laboratory and field data on immersion freezing was selected as
205 105% for the central lamina condition, or 5% supersaturation with respect to water. An
206 additional consideration in selecting this value is that RH_w uncertainty, as estimated and
207 extrapolated from Richardson (2009), is $\pm 1.6, 2$ and 2.4% at $-20, -25,$ and -30°C , respectively
208 (Hiranuma et al., 2014). Thus, a processing RH_w of 105% assures that particles are exposed to
209 a minimum RH_w of $\sim 102\%$ at the central lamina position, a value that should favor droplet
210 activation even for wettable particles at sizes exceeding the lower limit ($>0.1\ \mu\text{m}$) that typifies
211 most INPs on the basis of theoretical (Marcolli et al., 2007) and observational (DeMott et al.,
212 2010) studies.

213 Figure 2 also demonstrates a common feature noted in earlier studies of polydisperse
214 populations of both mineral dust (DeMott et al., 2011) and biomass burning aerosols (Petters
215 et al., 2009) acting as INPs, which is the asymptotic rise of INP active fraction when RH_w
216 exceeds 100%, up to the upper limit for droplet breakthrough. This result suggests that
217 unresolved factors are limiting the full expression/observation of immersion freezing

218 nucleation in the CFDC until relatively high water supersaturation. Extended discussion of
219 factors influencing this feature that require further research is given in Appendix B, but we
220 here follow Petters et al. (2009) in interpreting that the INP active fraction at high RH_w , prior
221 to droplet breakthrough, reflects the maximum INP activity achievable at a given CFDC
222 processing temperature for which all particles have been activated into cloud droplets and
223 diluted sufficiently to promote immersion freezing. Additional experimental support for the
224 fact that nearly complete CCN activation and growth of mineral dust particles occurs in the
225 CSU CFDC at RH_w between 105 and about 110% RH_w is given in Appendix B, Fig. B2. We
226 may contrast our assumptions and approach in this regard to that of Welts et al. (2014), who
227 used separate experiments to define immersion freezing fractions and then applied calculation
228 and subtraction methods to interpret and attribute additional INP fractions freezing as
229 contributions from a condensation freezing process at $RH_w > 100\%$.

230 **2.2 AIDA cloud chamber and data analysis**

231 The AIDA cloud simulation chamber is a large vessel with a volume of 84 m^3 that can be
232 sealed and evacuated to simulate cloud parcel expansion. It has been used extensively for ice
233 nucleation studies and specifically for investigations and parameterization of immersion
234 freezing nucleation (Niemand et al., 2012). Detailed descriptions of the device and
235 instrumentation are given in Möhler et al. (2006) and Wagner et al. (2006). Preparation of the
236 chamber for cloud expansions involves flushing with clean synthetic air to reduce particle
237 concentrations to below 0.1 cm^{-3} and using initial expansions to create a thin ice layer on the
238 chamber walls so that the relative humidity is close to ice saturation at the start temperature
239 for cloud expansions. Initial temperature is set by cooling the insulated box enclosure that
240 surrounds the stainless steel chamber. Locking and evacuating the chamber leads to adiabatic
241 temperature reduction within the chamber and cloud formation occurs once the humidity
242 exceeds 100% with respect to water. Temperature uncertainty is 0.2 K and uncertainty in
243 relative humidity with respect to ice is approximately 5%. The time length of cloud
244 expansions is ultimately limited by heat transfer into the cloud volume and sedimentation of
245 larger cloud particles.

246 Aerosols tested as ice nuclei are typically first generated into the 4 m^3 aerosol chamber before
247 being drawn into the AIDA chamber (Kanji et al., 2011). Dust samples were produced using
248 an RBG-1000 rotating brush disperser (Palas GmbH), while SnomaxTM bacteria were
249 generated using spray atomization and mixing with dry air. Ambient air can also be drawn

250 directly into the AIDA chamber. Total particle number concentration is measured
251 continuously using a condensation particle counter (CPC3010; TSI Inc.) and size distributions
252 are determined pre-expansion using a Scanning Mobility Particle Sizer (SMPS; TSI Inc.) and
253 an Aerodynamic Particle Sizer (APS, TSI Inc.). Cloud droplet and ice crystal counting and
254 sizing are achieved with two Welas optical particle counters (Palas GmbH) as described by
255 Benz et al. (2005).

256 Analysis of AIDA cloud expansion data in immersion freezing experiments follows Niemand
257 et al. (2012), as shown in Fig. 3. As for the CFDC, we interpret AIDA activation of natural
258 mineral dust INPs as occurring in a deterministic manner, although differences between the
259 two techniques could also reflect longer activation times at the modest cooling rates ($\sim 1\text{K}$
260 min^{-1} after cloud forms) in AIDA expansions. Figure 3 shows an expansion that followed the
261 CFDC sampling shown in Fig. 2. Full activation of aerosol into cloud droplets is achieved in
262 AIDA ($\pm 30\%$ maximum deviation, as noted by Niemand et al., 2012) and ice active fraction
263 of aerosol frozen exceeds 0.001 below about 250 K and 0.01 by 247 K, 4 minutes after cloud
264 formation. Note that we utilize AIDA data only up to the point that ice number concentrations
265 are still increasing, and so terminate analyses of ice active fraction beyond this point. Ice
266 crystals much larger than 100 μm can exist after this time, so that sedimentation begins to
267 become significant in the chamber, and this is a useful diagnostic for terminating the
268 attribution of INP number concentrations and active fraction to instantaneous temperature in
269 the chamber.

270 **2.3 Parameterization approach**

271 The D10 parameterization of a “global” type of INP collected from multiple locations took
272 the form,

$$273 \quad n_{INP}(T_k) = a(273.16 - T_k)^b (n_{a>0.5\mu\text{m}})^{(c(273.16 - T_k) + d)} \quad (1)$$

274 where $a = 0.0000594$, $b = 3.33$, $c = 0.0264$, $d = 0.0033$, T_k is cloud temperature in degrees
275 Kelvin, $n_{a>0.5\mu\text{m}}$ is the number concentration (std cm^{-3}) of aerosol particles with diameters
276 larger than 0.5 μm , and $n_{INP}(T_k)$ is ice nucleating particle number concentration (std L^{-1}) at T_k .

277 Tobo et al. (2013) proposed a modified version of Eq. (1) to more generally describe the size
278 and temperature dependence of various composition-specific types of INPs as, which we
279 modify slightly as,

280
$$n_{INP}(T_k) = (cf) (n_{a>0.5\mu m})^{(\alpha(273.16-T_k)+\beta)} \exp(\gamma(273.16-T_k) + \delta) \quad (2)$$

281 The cf factor was not included in Tobo et al. (2013), by default being set to 1. The other
282 equation coefficients could encapsulate this constant, but we will use it as a means to
283 segregate instrumental calibration factors when assessing maximum immersion freezing
284 concentrations or active fractions of mineral dust particles, as will be further addressed in this
285 paper. As for Eq. (1), the units of concentration in this equation are at standard temperature
286 and pressure conditions.

287 Less accurate predictability might be expected in relating $n_{INP}(T_k)$ to larger aerosol particle
288 concentrations rather than to aerosol surface area, which is expected to be a more natural
289 unifying factor as regards quantifying the ice nucleation ability of specific types of INPs
290 (Niemand et al., 2012; Murray et al., 2012; Knopf and Alpert, 2013). We evaluate this point
291 using atmospheric data, as discussed in the next section.

292 We apply Eq. (2) to describe INP number concentrations for a specific category taken to
293 represent all mineral dusts, a simplification we support with the existing data. Again, we will
294 also follow the approach of Petters et al. (2009) to quantify the maximum immersion freezing
295 activity of laboratory-generated mineral dust particles using CFDC data, in consideration of
296 instrumental and microphysical factors that lead to an RH_w dependence of INP number
297 concentrations above water saturation in CFDC-style instruments. This exercise defines a
298 single cf value. The derived cf value is applied to CFDC data collected on aerosols present
299 prior to cloud-forming expansions in the AIDA chamber in order to test consistency with ice
300 fractions formed in the laboratory supercooled clouds. We also compare Eq. (2) with the
301 active site density (INPs per surface area) parameterization for mineral dust INPs of Niemand
302 et al. (2012) for atmospheric measurements in a Saharan dust layer. This case is introduced in
303 the next section.

304 **2.4 Case study and other field data**

305 A case study from the ICE-T experiment was selected for use in comparing the developed
306 parameterization to the surface active site density parameterization of dust INP number
307 concentration (Niemand et al., 2012). The NSF/NCAR C-130 aircraft flew an instrument
308 package including meteorological and state parameter measurements, aerosol and cloud
309 microphysical wing-mounted probes, aerosol and gas phase sampling systems that used inlets
310 to the cabin (this included the CFDC), and the Wyoming cloud radar (WCR) and lidar (WCL)

311 instruments (Wang et al., 2012). The forward-facing isokinetic aerosol inlet used is the same
312 as described by Eidhammer et al. (2010). Concentrated African dust particle layers were
313 sampled on only a few days during the month-long ICE-T study. The case selected, from July
314 4, 2011 (called RF02 in the ICE-T data archive at NCAR) included perhaps the most
315 prominent elevated African dust layer that was sampled during the study. This case was quite
316 similar to the African dust layer case documented near Florida by DeMott et al. (2003), but
317 the CFDC processing conditions in the present case were selective for heterogeneous
318 immersion freezing, as already discussed. A vertical profile during descent through the dust
319 layer and into the marine boundary layer (MBL) is shown in Fig. 4. The dust layer is clearly
320 distinguished by the higher aerosol number concentrations and surface areas at sizes above
321 $0.5 \mu\text{m}$ measured by the wing-mounted FSSP-300 (Forward Scattering Spectrometer Probe –
322 300) at between 1300 and 4000 m altitude. This aerosol signature is not associated with
323 clouds, as evidenced by the lower relative humidity in this altitude range. The composition of
324 this elevated aerosol layer is inferred to be dominated by mineral dusts due to the prediction
325 of transported dust in the region by global aerosol forecast models (not shown) and by the
326 higher values of lidar linear depolarization ratio (LDR) measured by the WCL in the layer
327 above about 1300 m, as shown in Fig. 4. LDR, which is the ratio of perpendicular backscatter
328 intensities to parallel backscatter intensities with respect to the transmitter polarization axis, is
329 an excellent diagnostic for mineral dust (Sassen et al., 2003; Wang et al., 2009). Figure 4 thus
330 demonstrates a clear distinction between the mineral dust layer and the MBL below this level.
331 This transition in aerosol characteristics provides a stringent and informative case for testing
332 parameterizations of mineral dust INPs.

333 Other brief entries into the dust layers during ICE-T RF02 (July 4, 2011), and PACDEX G-V
334 flight data from RF12 (May 22, 2007) and RF14 (May 24, 2007) obtained while tracking a
335 cross-Pacific dust plume described by Stith et al. (2009), were used in the compilation of
336 CFDC data for parameterization development. Lidar data were not available during
337 PACDEX, and so identification of dust layers were primarily by the presence of larger
338 particles at higher altitudes in predicted plume regions (Stith et al., 2009).

339

340 **3 Results**

341 **3.1 Parameterization of CFDC INP data**

342 CFDC measurements of $n_{INP}(T_k)$ processed at 105% RH_w versus $n_{a>0.5\mu m}$, measured with the
343 CFDC optical particle counter, are shown in Fig. 5 at nominal 5 K temperature intervals. Data
344 collected while sampling particles aerosolized from Asian and Saharan soil sources into the
345 AIDA aerosol chamber are included together in Fig. 5 with field measurements made within
346 Saharan and Asian dust plumes. Laboratory data represent 1 to 3 minute average data while
347 field data are averaged over 5-30 minute periods, as per protocol used by DeMott et al.
348 (2010). Uncertainties represented by error bars on data points are twice the sampling error
349 assuming Poisson arrival statistics for CFDC INP counts. Figure 5 also shows that INP
350 number concentrations increase by approximately a factor of 10 per 5°C temperature interval
351 at any $n_{a>0.5\mu m}$. While differences of a factor of 2 to 3 are seen amongst different lab and field
352 aerosols for processing at one temperature, these results suggest that it is possible to
353 approximately unify the different data sets using Eq. (2). For example, plotted as dashed lines
354 in Fig. 5 is Eq. (2) with $cf = 1$, $\alpha = 0$, $\beta = 1.25$, $\gamma = 0.46$, and $\delta = -11.6$, considering all data
355 taken as one sample. As a reminder, cf is taken as 1 in this case because these are CFDC data
356 collected specifically at the reference RH_w value of 105%. Comparison of predicted versus
357 observed INP number concentrations for the entire data set are shown in Fig. 6. The r^2 of the
358 fit is 0.94, and the corresponding standard errors (a factor of ~2) and 95% confidence
359 intervals (a factor or ~4) are also shown. Representative standard errors at specific
360 temperatures are also mapped onto the predicted lines in Fig. 5. These analyses suggests that,
361 to first order, the INP activity of these dusts that surely contain gross mineralogical
362 differences can nevertheless be quantitatively described by the same relation for application in
363 a relatively simple form in numerical models.

364 This parameterization for mineral dust particles is compared to the D10 parameterization at
365 -30°C (243.2 K) and -20°C (253.2 K) in Fig. 7. At lower temperatures and higher dust number
366 concentrations, the D10 parameterization may strongly underestimate INP number
367 concentrations. However, the parameterizations are less distinguishable at certain warmer
368 temperatures and at lower values of $n_{a>0.5\mu m}$. Both parameterizations remain weakly
369 constrained at temperatures warmer than -20°C, where much additional ambient and
370 laboratory data are needed. The parameterization developed herein is strictly valid where data

371 were available, between 238 and 252 K, and use to warmer temperatures represents pure
372 extrapolation.

373 **3.2 Maximum active freezing fractions – derivation of calibration factor (*cf*)** 374 **and comparison to AIDA cloud expansions**

375 We utilized a number of additional CFDC experiments from the ACI03 campaign at a variety
376 of processing temperatures, while sampling of aerosols from the aerosol storage vessel, to
377 perform a comparison/calibration of the INP number concentration at maximum RH_w values
378 measured to $n_{INP}(T_k)$ at 105% RH_w . These results are shown in Fig. 8. The regression line in
379 Fig. 8 is drawn for the range of atmospherically realistic INP number concentrations,
380 primarily including data only to as low as -30°C , which are the conditions also used by
381 Niemand et al. (2012) to determine their surface area-based parameterization. The calibration
382 factor for maximum active fraction is approximately 3, and we suggest this value as the *cf*
383 prefactor in Eq. (2) for applying the parameterization to atmospheric data. We repeat the
384 caveat that the influences on the maximum INP number concentration values measured by the
385 CSU CFDC are not clearly resolved, and could mask a warm temperature bias to the fraction
386 of particles active at the steady-state processing temperature set in the CFDC (see Appendix
387 B). For this reason, comparison was sought versus ice formation data from AIDA cloud
388 expansion experiments, considered as ground truth for clouds.

389 For comparison of CFDC INP data with AIDA chamber experiment data, experiments were
390 utilized for which direct sampling of aerosol conditioned in the AIDA chamber was done with
391 the CFDC prior to first expansion cloud formation in ACI03 and ICIS studies. Additionally,
392 we considered only experiments for which the CFDC and AIDA cloud temperatures were
393 within 1°C of each other, or for which the CFDC processed at two temperatures to allow
394 linear interpolations of INP numbers and active fractions for comparison. These restrictions
395 limited the number of such comparisons available from sampling of INPs in past studies.

396 There were a total of eight experiments, listed in Table 1, for which a direct comparison of
397 CFDC maximum INP number concentration at a given temperature sampled from AIDA pre-
398 expansion, and equivalent immersion freezing INP concentration and active fraction from the
399 subsequent first AIDA expansions were available. Table 1 also notes the aerosol
400 concentration larger than $0.5\ \mu\text{m}$, as required for parameterization following Eq. (2), and total
401 aerosol surface area as required by the parameterization of Niemand et al. (2012). The INP

402 types represented in this comparison are Saharan (SD) and Asian dust (AD2), Canary Island
403 dust (CID), ambient particles (Amb), and sprayed/dried SnomaxTM bacterial particle
404 suspensions, as described by Niemand et al. (2012) and Kanji et al. (2011). In some cases, the
405 mineral dusts were coated by exposure to secondary organic aerosol formation (Kanji et al., in
406 preparation), noted as “cSOA” in Table 1. Comparison of active fractions from the two
407 instruments is shown in Fig. 9. General agreement is found between the measurement
408 methods, with a bias toward higher INP concentrations in AIDA for this small sample of
409 experiments.

410 In Figure 10, the mineral dust parameterization with $cf = 3$ in Eq. (2) is compared to the D10
411 parameterization to highlight the steeper activity dependence of mineral dust particles
412 compared to all types of INPs sampled to formulate D10. One might wonder if the cf factor
413 should be applied to the D10 measurements as well, but further measurements will be needed
414 to determine if corrections are valid for all the types of natural ice nuclei represented in the
415 D10 measurements at different temperatures. This is especially highlighted in Fig. 10 by the
416 fact that mineral dusts do not explain the INP activity suggested using the D10
417 parameterization at temperatures warmer than 253 K, at least for typical atmospheric $n_{a>0.5\mu m}$
418 of less than a few cm^{-3} . This is the temperature regime that may be dominated by organic ice
419 nucleating particles such as ice nucleating bacteria (Garcia et al., 2012; O’Sullivan et al.,
420 2014). It is also a temperature regime where more data were collected for D10 vs. very little
421 in the present work.

422 3.3 Case study intercomparison

423 It is clear that the new mineral dust parameterization should reasonably predict the CFDC
424 data observed in the Saharan Aerosol Layer profile during the RF02 flight in the ICE-T study,
425 since these data were included in the set used for developing the parameterization.
426 Nevertheless, the comparison is useful for evaluating the consistency or differences between
427 different INP parameterizations when applied for ambient aerosol data, including mineral dust
428 particle distributions extending to sizes $>2.5 \mu\text{m}$ that were not sampled into the CFDC. As
429 noted in Fig. 4, Saharan aerosols were focused within a layer overlying the marine boundary
430 layer, with total surface areas per unit volume exceeding $8 \times 10^{-11} \text{ m}^2 \text{ cm}^{-3}$ and number
431 concentrations as high as 30 cm^{-3} at sizes above $0.5 \mu\text{m}$ as measured by a forward scattering
432 spectrometer probe (FSSP-300, Droplet Measurement Technologies, Boulder, CO). Such

433 layers were not seen in aerosol vertical profiles or in lidar data on non-dusty days (not
 434 shown). INP number concentration data from the descent sounding through this layer is
 435 shown in Fig. 11, plotted as 30-s running average data instead of averages over an integrated
 436 period. Appropriate uncertainties are shown for this averaging interval at two representative
 437 altitudes and INP number concentrations. As repeat sampling of the layer was originally
 438 intended (but was instead terminated by early landing), CFDC sample flow was stopped for a
 439 short period during the stepped-descent (note data at ~3000 m and 700 m levels represent
 440 additional time spent at those levels) to remove an ice crystal impactor collecting activated
 441 particles, and then a period of filtering sample air was performed to quantify and correct for
 442 background counts that can potentially be generated through frost particle ejection from
 443 surfaces in the chamber (Prenni et al., 2009). This transition interrupted assessment of INP
 444 concentration through the depth of the layer, but since aerosol concentrations were
 445 continuously sampled by the FSSP-300, the parameterizations could be applied using CFDC
 446 sample temperatures during the balance of the descent. FSSP-300 number concentrations of
 447 particles at sizes above 0.5 μm were used within the mineral dust parameterization, while the
 448 FSSP-300 surface area was used within the Niemand et al. (2012) parameterization. For
 449 simplification, we apply that parameterization to the integrated aerosol surface area per unit
 450 volume (S_{tot} in $\text{m}^2 \text{cm}^{-3}$) at sizes above 0.5 μm to obtain $n_{INP}(T_k)$ in units per ambient liter as,

$$451 \quad n_{INP}(T_k) \approx 1 \times 10^{-3} S_{tot} n_s(T_k), \quad (3)$$

452 where $n_s(T_k)$ [m^{-2}] is given by Niemand et al. (2012) as,

$$453 \quad n_s(T_k) = \exp[-0.517(T_k - 273.15) + 8.934] \quad (4)$$

454 The approximation in Eq. (3) bypasses a usual need to bin surface area by particle size and
 455 integrate the terms within an exponential (c.f., Eq. (2) of Niemand et al., 2012). We consider
 456 it valid for the case shown in Fig. 11 because the contributions of aerosols larger than 5 μm
 457 were limited, and because the CFDC temperature used limits the total active fractions of
 458 particles in the size range below 5 μm to less than about 0.1, and hence binning surface area is
 459 not required for accuracy.

460 The results shown in Fig. 11 demonstrate several points. First, $n_{INP}(T_k)$ as measured by the
 461 CFDC while processing at 105% RH_w is well reproduced by the new mineral dust
 462 parameterization (Eq. (2) with $cf = 1$ (trace “D” in Fig. 11) within the Saharan aerosol layer.
 463 This is to be expected on the basis of the parameterization development in Section 3.1, where

464 $cf = 1$ represents uncorrected data. However, in the marine boundary layer, CFDC IN data are
465 already grossly overestimated by the uncorrected mineral dust parameterization ($cf = 1$), and
466 even appear overestimated by the global IN parameterization (D10). This result suggests that
467 the aerosol and INPs in the marine boundary layer are quite distinct from the Saharan aerosol
468 layer, which has not been well-mixed into the marine boundary layer at the location of
469 measurements. Within the mineral dust layer, the corrected form of the parameterization using
470 $cf = 3$ is in excellent agreement with the Niemand et al. (2012) parameterization (trace “N12”)
471 for this case. While providing confidence that both parameterizations can thus be used to
472 describe atmospheric ice nucleation by mineral dust particles specifically in the temperature
473 ranges for which they were developed, we note that comparison to ice formation in
474 atmospheric clouds has yet to be examined.

475

476 **4 Conclusions**

477 A parameterization based on a combination of laboratory and field data was developed to
478 specifically quantify the immersion freezing numbers of natural mineral dust particles. This
479 parameterization links the prediction of ice nucleating particle number concentrations to
480 particle number concentrations at sizes larger than $0.5 \mu\text{m}$ and to temperature, but is specific
481 to mineral dust compositions. In this manner, the higher efficiency of mineral dust particles in
482 comparison to global-average INPs at temperatures colder than -20°C is quantified for use in
483 numerical models. Use of the parameterization to warmer temperatures necessarily entails
484 extrapolation of the present results. Agreement was found between this simplified
485 parameterization and the surface area based parameterization of Niemand et al. (2012),
486 developed solely from laboratory data, supporting the atmospheric applicability of laboratory
487 ice nucleation results to the atmosphere. Consequently, our results additionally support the
488 premise of Niemand et al. (2012) that, to a first order, mineral dust particles from locations as
489 separate as the Saharan or Asian regions may be parameterized as a common particle type for
490 numerical modeling purposes. The reason for this result is not entirely clear, given the clear
491 mineralogical differences present in and transported from different desert regions (Murray et
492 al., 2012). Possibly, the relatively high abundance ($>20\%$ by mass) of more highly ice-active
493 specific components of dusts, such as feldspars, from both Asian and Saharan regions
494 (Atkinson et al., 2013) drives this result. Nevertheless, it remains to be seen that this
495 conclusion is fully consistent with the unifying role of aerosol concentrations at $>0.5 \mu\text{m}$ or

496 total surface area of mineral dust particles on determining INP number concentrations, since
497 many other mineral components make up the balance of dust particle mass. It remains for
498 additional measurements at different locales to further evaluate this conclusion regarding the
499 relative uniformity of INP properties of mineral dust particles globally or, alternately, to
500 demonstrate the special utility of mineralogical-specific parameterizations. It is also necessary
501 to point out that we have not herein explicitly considered or evaluated the potential impact of
502 aging processes (e.g., uptake condensed phase material) or cloud processing on the measured
503 or predicted immersion freezing activity. Such impacts may or may not already be present in
504 the field measurements. Some of the laboratory experiments included particle coatings with
505 secondary organic aerosol, which appeared to have no significant impact on immersion
506 freezing (to be elaborated in a future publication). Additionally, we may note that a number of
507 previous studies suggest little influence of aging on immersion freezing of activated cloud
508 droplets by mineral dusts, unless reactions occur between the condensed species and the
509 mineral surface that impact the efficiency of active sites (Sullivan et al., 2010a, 2010b;
510 Niedermeier et al., 2011a; Reitz et al., 2012).

511 Our investigations support that a calibration factor on CFDC INP concentrations is needed to
512 account for instrumental factors if the intent is to describe the full expression of
513 condensation/immersion freezing by natural mineral dust particles. The CFDC processing
514 RH_w value that is required for such full expression may exceed that practically possible for
515 use while measuring ambient aerosol size distributions (e.g., without achieving droplet
516 breakthrough contamination of the ice nucleation signal), so further laboratory studies may be
517 required for specific INP aerosol types. We suggest $cf = 3$ for predicting $n_{INP}(T_k)$ for
518 immersion freezing by natural mineral dusts using Eq. (2), along with the other
519 parameterization coefficients that have been obtained based on sampling at a practical RH_w of
520 105%. While the calibration factor did not depend on processing temperature for the mineral
521 dust particles examined, and has been shown to likely be necessary for fully quantifying INPs
522 from biomass burning particles (Petters et al. 2009), cf and the form of this composition-
523 specific parameterization may be specific to the type of INP. For example, SnomaxTM INPs
524 are fully activated in a CFDC by the point of water saturation at all temperatures below about
525 -7°C (see, e.g., DeMott et al., 2011), and so no further activation occurs in the supersaturated
526 regime. A data point for such an experiment is shown in Fig. 9, and consequently is a positive
527 outlier of CFDC/AIDA active fraction after application of $cf = 3$. Nevertheless, these results
528 have implications for the design and operation of any CFDC-type ice nucleation instrument,

529 suggesting careful characterization of ice nucleation response to RH_w for any particular
530 device and different INP types that compose natural populations. In particular, scanning up to
531 and beyond the RH_w for droplet breakthrough to establish CCN activation (e.g., Fig. B2) is
532 recommended. This will more clearly define the upper RH_w limit for assessing ice active
533 fraction versus temperature uniformly for any INP type being tested and CFDC instrument
534 type being used.

535 Use of Eq. (2) to describe condensation/immersion freezing nucleation will depend on
536 accurate prediction of where dust particles are present and where they are not, as the gross
537 over-prediction of INPs for the tropical marine boundary layer aerosols shown in Fig. 11
538 demonstrates. Finally, in applying the parameterization in cloud models, consideration may
539 need to be given to CCN activation properties (i.e., particles must be in droplets) and loss of
540 INPs to wet scavenging that occurs prior to cloud parcels reaching freezing temperatures. A
541 first application of the new parameterization in a prognostic ice nucleation scheme within
542 regional model simulations has been published by Fan et al. (2013).

543

544 **Appendix A**

545 **A brief discussion of deterministic versus stochastic analyses and parameterization**

546 The approach in this paper follows the deterministic (or singular) interpretation of immersion
547 freezing data, which approximates immersion freezing as temperature-dependent only and
548 does not quantify time-dependent ice nucleation behavior. This is in contrast to a purely
549 stochastic model or to multi-component stochastic models designed to quantify the time-
550 dependent characteristics of INPs, as summarized for example in Niedermeier et al. (2011b),
551 Murray et al. (2012), Wright and Petters (2013), Knopf and Alpert (2013) and Vali (2014). In
552 a deterministic approach, one primarily seeks to define the ice nucleation activity spectrum
553 measured during a set instrument time or using a set cooling rate, represented by a relation
554 between INP number concentrations and temperature for a known total number (e.g., DeMott
555 et al., 2010) or surface area (e.g., Niemand et al., 2012; Hoose and Moehler, 2012; Murray et
556 al. 2012) of particles. Wright and Petters (2013) and Vali (2014) discuss the fact that
557 temperature dependence dominates time dependence for most INP types. An expectation of
558 the applicability of the singular approximation for freezing of natural mineral dusts follows
559 Broadley et al. (2012), wherein NX-Illite is proposed as a surrogate for airborne mineral dust,
560 and such particles show little dependence of ice nucleation rate on cooling rate. Finally,

561 Wright and Petters (2013) specifically conclude that a CFDC should represent INP
562 concentrations active in updrafts, despite the short observational time for detecting INPs. This
563 is because the additional nuclei active over time at any supercooled temperature are typically
564 found to represent those newly active for an additional 1 to 3K cooling. This fact may in
565 many cases simplify numerical model prediction of ice formation, as tracking the budget of an
566 INP population undergoing variable nucleation rates can be difficult to implement in a
567 prognostic cloud model. Deterministic interpretation also involves the most straightforward
568 use of data collected by real-time ice nucleation instruments, and future reanalyses for
569 nucleation rates is still possible.

570 Knopf and Alpert (2013) also quantify the relation of immersion freezing nucleation rate to
571 water activity, and thus that parameterization unifies heterogeneous immersion freezing for
572 both cloud droplets and non-dilute haze particles that may freeze below water saturation at
573 lower temperatures. In a similar manner, Sassen and Dodd (1988) and DeMott et al. (1997;
574 1998) beforehand applied the concept of effective freezing temperature versus solution
575 melting point depression to adjust deterministically-analyzed freezing data for INPs immersed
576 in dilute droplets to conditions of more concentrated solution droplets. Thus, deterministic
577 models may presumably be formulated to account for the now recognized water activity
578 dependence of freezing as well. Nevertheless, as already mentioned, this papers focuses on
579 the first order data needed, the ice nucleation activity temperature spectrum for INPs within
580 pure water droplets.

581

582 **Appendix B**

583 **Additional discussion of factors affecting INP activation above water saturation in** 584 **CFDC instruments**

585 In the analyses presented in this paper, the *cf* factor in Eq. (2) is defined by assuming that
586 immersion freezing INP number concentrations for mineral dust particles are underestimated
587 at the CFDC reference RH_w value of 105%, in which case a higher RH_w value is required to
588 fully activate immersion freezing on the entire aerosol distribution. The need to achieve
589 higher RH_w , as shown in Figure 2, likely relates to both microphysical and instrumental
590 factors that play interwoven roles, with consequent implications for operating CFDC
591 instruments and interpreting their data (DeMott et al., 2011). While this discussion is

592 generally applicable to all CFDC-type instruments, it is specific to the configuration of the
593 CSU CFDC, and results will be different for other similar instruments.

594 First, if the CFDC exposed all particles to the same conditions for the same amount of time,
595 independent of RH_w , then we should expect a nearly delta-function response of INP number
596 fraction to RH_w ensuing around the RH_w values that characterize CCN activation. For mineral
597 dust particles, hygroscopicity is thought to be low (Koehler et al., 2009; Herich et al., 2009),
598 but may be mitigated by adsorption activation (Kumar et al., 2009), such that a range of
599 critical supersaturations from a few tenths of a percent to perhaps 1-2% for smaller particles
600 could be imagined as an inherent kinetic delay for condensation/immersion freezing in the
601 CFDC. There may be kinetic factors as well related to diluting any condensed material away
602 from ice active sites on mineral particle surfaces.

603 However, in addition to activation effects, the CFDC method neither assures equal exposure
604 of RH_w nor equal time of immersion of potential INPs in cloud particles at varied RH_w .
605 Again, Fig. 1 shows the dynamic changes in temperature and SS_w that occur prior to a short
606 period of nearly steady state conditions that characterize CFDC-type instruments. It is also
607 apparent from Fig. 1 that for a steady flow rate, the time of existence of droplets exceeding a
608 certain size, e.g. 1 μm , increases with RH_w . Dynamic consideration given to altering flow rate
609 would be needed in order to maintain the residence time of particles in droplets at the same
610 value for different processing RH_w . The discussion given in Section 2.1 was simplified to
611 focus on the central conditions of the CFDC aerosol lamina. However, RH_w conditions across
612 the aerosol lamina at any one position during transit of particles through the CFDC are also
613 variable. As shown in Fig. B1a the edge-to-edge RH_w difference across the aerosol lamina is
614 2% for an RH_w “set point” of 105% at -30°C . That RH_w difference exists for perfect
615 containment of the aerosol inside the lamina, which may not be achieved operationally, as
616 discussed originally by Rogers (1988). Figure B1b revisits this topic, showing recent
617 measurements of the transit of a 1 s particle pulse through the CFDC. Comparison of the
618 predicted time of this particle pulse versus that observed by monitoring the particle number
619 concentration at the CFDC outlet with a condensation particle counter indicate skewing of the
620 timing of the pulse, suggesting a range of pass-through times for particles. These results
621 indicate that although particles are retained mainly within the position of the aerosol stream,
622 some particles likely escape the central lamina to a distance of up to 4 times the lamina
623 breadth. This potential spread in lamina thickness is highlighted by shading in Fig. B1a. Since

624 we do not know the true distribution of particles in this space, we will not pursue a
625 quantitative example here, but it is obvious that a spread of particles, especially toward the
626 cold wall, leads to a wide range of RH_w exposure of some proportion of particles for a steady
627 state target RH_w above water saturation. Only at much higher target supersaturation will the
628 entire lamina reside above water saturation, although this will necessarily increase the breadth
629 of representative temperatures. This could be the most important factor affecting the detection
630 of condensation/immersion freezing nucleation of natural mineral dust particles with a CFDC.
631 Despite these concerns, evidence clearly exists for high CCN active fractions ultimately
632 occurring in the CSU CFDC instrument for RH_w values close to the values used to define the
633 maximum immersion freezing INP concentrations in these studies. Figure B2 shows two
634 additional experiments from the ICIS-2007 studies where RH_w was raised to higher values to
635 examine full droplet breakthrough, indicating CCN fractions up to 0.8. Similar freezing
636 curves occurring for homogeneous freezing of solution droplets have also been previously
637 demonstrated for the CSU CFDC instruments (DeMott et al., 2009; Koehler et al., 2009;
638 Richardson, 2009; Richardson et al., 2010), indicating no special limitation on freezing high
639 fractions of particles in these instruments. These results support the validity of the assumption
640 that immersion freezing activity is assessed with the CFDC instrument in the present study.

641 It is also necessary to mention the additional cooling that droplets are exposed to during entry
642 into and persistence through the CFDC evaporation section as a possible positive artifact
643 leading to enhanced ice activation as RH_w is increased. Evaporation is forced by setting both
644 ice walls to the colder ice wall temperature in the CSU CFDC design. The temperature curve
645 in Fig. 1 shows that droplets do not evaporate until temperature has decreased by 2°C for
646 processing conditions of -30°C and $102\% RH_w$, while at $105\% RH_w$ and higher, droplets do
647 not completely evaporate during cooling by an additional 3°C before exit from the chamber to
648 the optical counter. Above about $105\% RH_w$, these droplets may stay dilute and the
649 consequence is that additional freezing could occur for this reason alone. Crystals nucleating
650 in this region will grow only slowly from their original droplet size, typically less than $1\ \mu\text{m}$
651 s^{-1} , due to the lowered ice supersaturation present. Thus, only at the highest RH_w approaching
652 water droplet breakthrough would late-forming crystals even have the possibility to exceed
653 the ice cut-size for detection as IN. Nevertheless, we must necessarily treat this factor as a
654 caveat concerning the corrections to ice active fraction that we propose on the assumption that
655 INP number concentration values measured at high RH_w are relevant for immersion freezing
656 at the CFDC steady state temperature.

657 Time-dependent immersion freezing could be considered as another possible source
658 explaining increasing ice activation versus RH_w . Inspection of Fig. 1 suggests a tripling of the
659 residence time for droplets larger than $1\ \mu\text{m}$ for an RH_w increase from 102 to 109%, whereas
660 Fig. 2 shows an ice active fraction increase of nearly an order of magnitude over this RH_w
661 range, suggesting that time dependence is not the primary factor at play. Nevertheless, we
662 note again that an analysis of data in terms of nucleation rates has not been performed here, as
663 the target format of the present parameterization is a time-independent form.

664 These characteristics of continuous flow chambers suggest the need for further investigation,
665 numerically and experimentally, to clarify the specific conditions and residence times
666 attributable to observed ice formation for different types of INP. INP detection may also be
667 influenced by how different CFDC-style devices drive reduction to ice saturation, for example
668 via reduction to the cold wall temperature (Rogers et al., 2001) or to the warm wall
669 temperature (Stetzer et al., 2008). The potential for particles to spread out of the intended
670 focused lamina and the consequent overall range of processing temperatures and RH_w
671 represented, probably depends critically on internal design of the aerosol delivery to the
672 center of the processing chamber. In general, these factors reemphasize the point that ice
673 nucleation devices do not yet operate to the potential precision of CCN devices and therefore
674 require careful consideration when evaluating things like apparent time dependence for ice
675 nucleation or ascribing meaning to the RH_w dependence of ice nucleation at above water
676 saturation by different INPs.

677

678 **Acknowledgements**

679 This work was partially funded by the National Science Foundation under grants ATM-
680 0611936, ATM-0841602 and AGS-1036028, and the Department of Energy, Office of
681 Science, Office of Biological and Environmental Research program under Contract #
682 SC00002354. J. Snider and Z. Wang acknowledge support under NSF award AGS-1034858.
683 Experiments performed at the Karlsruhe Institute of Technology (KIT) AIDA chamber were
684 supported by the Helmholtz Association through the Virtual Institute on Aerosol-Cloud
685 Interactions (VI-ACI, VH-VI-233) and the research program Atmosphere and Climate
686 (ATMO). P. DeMott also acknowledges KIT for supporting his visit to assist completion of
687 this paper. All processed data are available upon request.

688

689 **References**

- 690 Atkinson, J. D., Murray, B. J., Woodhouse, M. T., Whale, T. F., Baustian, K. J., Carslaw, K.
691 S., Dobbie, S., O’Sullivan, D., and Malkin, T. L.: The importance of feldspar for ice
692 nucleation by mineral dust in mixed-phase clouds, *Nature*, 498, 355–358, 2013.
- 693 Benz, S., Megahed, K., Möhler, O., Saathoff, H., Wagner, R., and Schurath, U.: T-dependent
694 rate measurements of homogeneous ice nucleation in cloud droplets using a large atmospheric
695 simulation chamber. *J. Photochem. Photobiol.*, 176, 208–217,
696 doi:10.1016/j.jphotochem.2005.08.026, 2005.
- 697 Broadley, S. L., Murray, B. J., Herbert, R. J., Atkinson, J. D., Dobbie, S., Malkin, T. L.,
698 Condcliffe, E., and Neve, L.: Immersion mode heterogeneous ice nucleation by an illite rich
699 powder representative of atmospheric mineral dust, *Atmos. Chem. Phys.*, 12, 287–307,
700 doi:10.5194/acp-12-287-2012, 2012.
- 701 DeMott, P.J., Kreidenweis, S. M., and Rogers, D. C.: The susceptibility of ice formation in
702 upper tropospheric clouds to insoluble aerosol components. *J. Geophys. Res.*, 102, 19575-
703 19584, 1997.
- 704 DeMott P.J., Rogers, D. C., Kreidenweis, S. M., Chen, Y., Twohy, C. H., Baumgardner, D.
705 Heymsfield, A. J., and Chan., K. R.: The role of heterogeneous freezing nucleation in upper
706 tropospheric clouds: Inferences from SUCCESS, *Geophys. Res. Lett.*, 25, 1387-1390, 1998.
- 707 DeMott, P. J., Sassen, K., Poellot, M. Baumgardner, D., Rogers, D. C., Brooks, S., Prenni A.
708 J., and Kreidenweis, S. M.: African dust aerosols as atmospheric ice nuclei. *Geophys. Res.*
709 *Lett.*, 30, No. 14, 1732, doi:10.1029/2003GL017410, 2003 (Correction published: *Geophys.*
710 *Res. Lett.*, 36, L07808, doi:10.1029/2009GL037639, 2009).
- 711 DeMott, P. J., Petters, M. D., Prenni, A. J., Carrico, C. M., Kreidenweis, S. M., Collett, J. L.
712 Jr., and Moosmüller, H.: Ice nucleation behavior of biomass combustion particles at cirrus
713 temperatures, *J. Geophys. Res.*, 114, D16205, doi:10.1029/2009JD012036, 2009.
- 714 DeMott, P.J., Prenni, A. J., Liu, X., Petters, M. D., Twohy, C. H., Richardson, M. S.,
715 Eidhammer, T., Kreidenweis, S. M., and Rogers, D. C.: Predicting global atmospheric ice
716 nuclei distributions and their impacts on climate, *Proc. Natnl. Acad. Sci.*, 107 (25), 11217-
717 11222, 2010.

718 DeMott, P. J., Möhler, O., Stetzer, O., Vali, G., Levin, Z., Petters, M. D., Murakami, M.,
719 Leisner, T., Bundke, U., Klein, H., Kanji, Z., Cotton, R., Jones, H., Benz, S., Brinkmann, M.,
720 Rzesanke, D., Saathoff, H., Nicolet, M., Saito, A., Nillius, B., Bingemer, H., Abbatt, J.,
721 Ardon, K., Ganor, E., Georgakopoulos, D. G., and Saunders, C.: Resurgence in ice nucleation
722 research. *Bull. Amer. Meteor. Soc.*, 92, 1623-1635, 2011.

723 Eidhammer, T., DeMott, P. J., Prenni, A. J., Petters, M. D., Twohy, C. H., Rogers, D. C.,
724 Stith, J., Heymsfield, A., Wang, Z., Haimov, S., French, J., Pratt, K., Prather, K., Murphy, S.,
725 Seinfeld, J., Subramanian, R., and Kreidenweis, S. M.: Ice initiation by aerosol particles:
726 Measured and predicted ice nuclei concentrations versus measured ice crystal concentrations
727 in an orographic wave cloud. *J. Atmos. Sci.*, 67, 2417–2436. doi: 10.1175/2010JAS3266.1,
728 2010.

729 Fan, J., Leung, L. R., DeMott, P. J., Comstock, J. M., Singh, B., Rosenfeld, D., Tomlinson, J.
730 M., White, A., Prather, K. A., Minnis, P., Ayers, J. K., and Min, Q.: Aerosol impacts on
731 California winter clouds and precipitation during CalWater 2011: local pollution vs. long-
732 range transported dust, *Atmos. Chem. Phys. Discuss.*, 13, 19921–19970, 2013.

733 Garcia, E., Hill, T. C. J., Prenni, A. J., DeMott, P. J., Franc, G. D., and Kreidenweis, S. M.:
734 Biogenic ice nuclei in boundary layer air over two U.S. High Plains agricultural regions, *J.*
735 *Geophys. Res.* 117, D18209, doi:10.1029/2012JD018343, 2012.

736 Herich, H., Tritscher, T., Wiacek, A., Gysel, M., Weingartner, E., Lohmann, U.,
737 Baltensperger, U., and Cziczo, D. J.: Water uptake of clay and desert dust aerosol particles at
738 sub- and supersaturated water vapor conditions, *Physical Chemistry Chemical Physics*, 11,
739 7804–7809, 2009.

740 Heymsfield, A. J., and Willis, P. T.: Conditions favoring secondary ice production in tropical
741 maritime convective clouds, Accepted to *J. Atmos. Sci.*, 2014.

742 Hiranuma, N. et al.: *Supplement of: A comprehensive laboratory study on the immersion*
743 *freezing behavior of illite NX particles: a comparison of seventeen ice nucleation*
744 *measurement techniques*, Supplement of *Atmos. Chem. Phys. Discuss.*, 14, 22045–22116,
745 doi:10.5194/acpd-14-22045-2014-supplement, 2014.

746 Kanji, Z., DeMott, P. J., Möhler, O., and Abbatt, J. P. D.: Results from the University of
747 Toronto Continuous Flow Diffusion Chamber at International Workshop on Comparing Ice
748 Nucleation Measuring Systems (ICIS 2007), *Atmos. Chem. Phys.*, 11, 31–41, 2011.

749 Knopf, D. A., and Alpert, P. A.: A water activity based model of heterogeneous ice nucleation
750 kinetics for freezing of water and aqueous solution droplets, *Faraday Discussions*, 165, 513-
751 534, DOI: 10.1039/C3FD00035D2013, 2013.

752 Koehler, K. A., Kreidenweis, S. M., DeMott, P. J., Petters, M. D., Prenni, A. J., and Carrico,
753 C. M.: Hygroscopicity and cloud droplet activation of mineral dust aerosol. *Geophys. Res.*
754 *Lett.*, 36, L08805, doi:10.1029/2009GL037348, 2009.

755 Koehler, K. A., DeMott, P. J., Kreidenweis, S. M., Popovicheva, O. B., Petters, M. D.,
756 Carrico, C., Kireeva, E., Khokhlova, T., and Shonija, N: Cloud condensation nuclei and ice
757 nucleation activity of hydrophobic and hydrophilic soot particles, *Phys. Chem. Chem. Phys.*,
758 11, 7906 – 7920, 2009.

759 Kumar, P., Nenes, A., and Sokolik I. N.: Importance of adsorption for CCN activity and
760 hygroscopic properties of mineral dust aerosol, *Geophys. Res. Lett.*, 36, L24804,
761 doi:10.1029/2009GL040827, 2009.

762 Marcolli, C., Gedamke, S., Peter, T., and Zobrist, B.: Efficiency of immersion mode ice
763 nucleation on surrogates of mineral dust, *Atmos. Chem. Phys.*, 7, 5081–5091,
764 doi:10.5194/acp-7-5081-2007, 2007.

765 Möhler, O., Field, P. R., Connolly, P., Benz, S., Saathoff, H., Schnaiter, M., Wagner, R.,
766 Cotton, R., Krämer, M., Mangold, A., and Heymsfield, A. J.: Efficiency of the deposition
767 mode ice nucleation on mineral dust particles. *Atmos. Chem. Phys.*, 6, 3007–3021,
768 doi:10.5194/acp-6-3007-2006, 2006.

769 Murray, B. J, O'Sullivan, D., Atkinson, J.D., and Webb, M. E.: Ice nucleation by particles
770 immersed in supercooled cloud droplets. *Chem. Soc. Rev.*, 41, 6519-6554, 2012.

771 Niedermeier, D., Hartmann, S., Clauss, T., Wex, H., Kiselev, A., Sullivan, R. C., DeMott, P.
772 J. Petters, M. D., Reitz, P., Schneider, J., Mikhailov, E., Sierau, B., Stetzer, O., Reimann, B.,
773 Bundke, U., Shaw, R. A., Buchholz, A., Mentel, T. F., and Stratmann, F.: Experimental study
774 of the role of physicochemical surface processing on the IN ability of mineral dust particles.
775 *Atmos. Chem. Phys.*, 11, 11131-11144, 2011a.

776 Niedermeier, D., R. A. Shaw, S. Hartmann, H. Wex, T. Clauss, J. Voigtländer and F.
777 Stratmann, Heterogeneous ice nucleation: exploring the transition from stochastic to singular
778 freezing behaviour, *Atmos. Chem. Phys.*, 11, 8767–8775, 2011b.

779 Niemand, M., Moehler, O., Vogel, B., Vogel, H., Hoose, C., Connolly, P., Klein, H.,
780 Bingemer, H., DeMott, P., Skrotzki, J., and Leisner, T.: Parameterization of immersion
781 freezing on mineral dust particles: An application in a regional scale model. *J. Atmos. Sci.*,
782 69, 3077-3092, 2012.

783 O'Sullivan, D., Murray, B. J., Malkin, T. L., Whale, T. F., Umo, N. S., Atkinson, J. D., Price,
784 H. C., Baustian, K. J., Browse, J., and Webb, M. E.: Ice nucleation by fertile soil dusts:
785 relative importance of mineral and biogenic components, *Atmos. Chem. Phys.*, 14, 1853–
786 1867, doi:10.5194/acp-14-1853-2014, 2014.

787 Petters, M. D., Parsons, M. T., Prenni, A. J., DeMott, P. J., Kreidenweis, S. M., Carrico, C.
788 M., Sullivan, A. P., McMeeking, G. R., Levin, E., Wold, C. E., Collett, J. L. Jr., and
789 Moosmüller, H.: Ice nuclei emissions from biomass burning. *J. Geophys. Res.*, 114, D07209,
790 doi: 10.1029/2008JD011532, 2009.

791 Phillips, V. T. J., DeMott, P. J., Andronache, C., Pratt, K., Prather, K. A., Subramanian, R.,
792 and Twohy, C.: Improvements to an Empirical Parameterization of Heterogeneous Ice
793 Nucleation and its Comparison with Observations. *J. Atmos. Sci.*, 70, 378-409, 2013.

794 Phillips, V. T. J., DeMott, P. J., and Andronache, C.: An Empirical Parametrisation of
795 Heterogeneous Ice Nucleation for Multiple Chemical Species of Aerosol. *J. Atmos. Sci.*, 65,
796 2757-2783, 2008.

797 Prenni, A. J., Petters, M. D., Faulhaber, A., Carrico, C. M., Ziemann, P. J., Kreidenweis, S.
798 M., and DeMott, P. J.: Heterogeneous ice nucleation measurements of secondary organic
799 aerosol generated from ozonolysis of alkenes, *Geophys. Res. Lett.*, 36, L06808,
800 doi:10.1029/2008GL036957, 2009.

801 Richardson, M. S., 2009: Making Real Time Measurements of Ice Nuclei Concentrations at
802 Upper Tropospheric Temperatures: Extending the Capabilities of the Continuous Flow
803 Diffusion Chamber, Ph.D Dissertation, Colorado State University, 262 pp.

804 Richardson, M. S., DeMott, P. J., Kreidenweis, S. M., Petters, M. D., and Carrico, C. M.,
805 2010: Observations of ice nucleation by ambient aerosol in the homogeneous freezing regime.
806 *Geophys. Res. Lett.*, 37, L04806, doi:10.1029/2009GL041912.

807 Reitz, P., Spindler, C., Mentel, T. F., Poulain, L., Wex, H., Mildenerger, K., Niedermeier,
808 D., Hartmann, S., Clauss, T., Stratmann, F., Sullivan, R. C., DeMott, P. J., Petters, M. D.,
809 Sierau, B., and Schneider, J.: Surface modification of mineral dust particles by sulphuric acid

810 processing: implications for ice nucleation abilities. *Atmos. Chem. Phys.*, 11, 7839-7858,
811 2011.

812 Rogers, D. C.: Development of a continuous flow thermal gradient diffusion chamber for ice
813 nucleation studies. *Atmos. Res.*, 22, 149–181, 1988.

814 Rogers, D.C., DeMott, P. J., Kreidenweis S. M., and Chen, Y.: A continuous flow diffusion
815 chamber for airborne measurements of ice nuclei, *J. Atmos. Oceanic Technol.*, 18, 725-741,
816 2001.

817 Sassen, K., DeMott, P. J., Prospero, J., and Poellot, M. R.: Saharan dust storms and indirect
818 aerosol effects on clouds: CRYSTAL-FACE results, *Geophys. Res. Lett.*, 30, No. 12, 1633,
819 doi:10.1029/2003GL017371, 2003.

820 Seifert, P., Ansmann, A., Groß, S., Freudenthaler, V., Heinold, B., Hiebsch, A., Mattis, I.,
821 Schmidt, J., Schnell, F., Tesche, M., Wandinger, U., and Wiegner, M.: Ice formation in
822 ash-influenced clouds after the eruption of the Eyjafjallajökull volcano in April 2010, *J.*
823 *Geophys. Res.*, 116, D00U04, doi:10.1029/2011JD015702, 2011.

824 Stetzer, O., Baschek, B., Lüönd, F., and Lohmann, U.: The Zurich Ice Nucleation Chamber
825 (ZINC)—A new instrument to investigate atmospheric ice formation. *Aerosol Sci. Technol.*,
826 42, 64–74, 2008

827 Stith, J. L., Ramanathan, V., Cooper, W. A., Roberts, G., DeMott, P. J., Carmichael, G.,
828 Hatch, C. D., Adhikary, B., Twohy, C. H., Rogers, D. C., Baumgardner, D., Prenni, A. J.,
829 Campos, T., Gao, R. S., Anderson, J., and Feng, Y.: An overview of aircraft observations
830 from the Pacific Dust Experiment campaign. *J. Geophys. Res.*, 114, D05207,
831 doi:10.1029/2008JD010924, 2009.

832 Sullivan, R. C., Petters, M. D., DeMott, P. J., Kreidenweis, S. M., Wex, H., Niedermeier, D.,
833 Stratmann, F., Reitz, P., and Schneider, J.: Irreversible loss of ice nucleation surface sites in
834 mineral dust particles induced by sulphuric acid condensation. *Atmos. Chem. Phys.*, 10,
835 11471-11487, 2010a.

836 Sullivan, R. C., Miñambres, L., DeMott, P. J., Prenni, A. J., Carrico, C. M., Levin, E. J.T.,
837 and Kreidenweis, S. M.: Chemical processing does not always impair heterogeneous ice
838 nucleation of mineral dust particles. *Geophys. Res. Lett.*, 37, L24805,
839 doi:10.1029/2010GL045540, 2010.

840 Tobo, Y., Prenni, A. J., DeMott, P. J., Huffman, J. A., McCluskey, C. S., Tian, G., Pöhlker,
841 C., Pöschl, U., and Kreidenweis, S. M.: Biological aerosol particles as a key determinant of
842 ice nuclei populations in a forest ecosystem, *J. Geophys. Res. - Atmos.*, DOI:
843 10.1002/jgrd.50801, in press 2013.

844 Vali, G., Interpretation of freezing nucleation experiments: singular and stochastic; sites and
845 surfaces, *Atmos. Chem. Phys.*, 14, 5271–5294, 2014.

846 Vali, G., Nucleation Terminology, *Bull. Am. Meteorol. Soc.*, 66, 1426–1427, 1985.

847 Wagner, R., Benz, S., Möhler, O., Saathoff, H., and Schurath, U.: Probing ice clouds by
848 broadband mid-infrared extinction spectroscopy: case studies from ice nucleation experiments
849 in the AIDA aerosol and cloud chamber. *Atmos. Chem. Phys.*, 6 (12), 4775–4800,
850 doi:10.5194/acp-6-4775-2006, 2006.

851 Wang, Z., Wechsler, P., Kuestner, W., French, J., Rodi, A., Glover, B., Burkhart, M., and
852 Lukens, D., Wyoming Cloud Lidar: instrument description and applications, *Optics Express*
853 Vol. 17, Iss. 16, pp. 13576–13587, 2009.

854 Wang, Z., French, J., Vali, G., Wechsler, P., Haimov, S., Rodi, A., Deng, M., Leon, D.,
855 Snider, J., Peng, L., and Pazmany, A. L.: Single aircraft integration of remote sensing and in
856 situ sampling for the study of cloud microphysics and dynamics. *BAMS*, 93, 653–766. doi:
857 10.1175/BAMS-D-11-00044.1, 2012.

858 Welti, A., Kanji, Z., Luound, F., Stetzer, O., and Lohmann, U.: Exploring the Mechanisms of
859 Ice Nucleation on Kaolinite: From Deposition Nucleation to Condensation Freezing, *J.*
860 *Atmos. Sci.*, 71, 16-36, 2014.

861 Wex, H., DeMott, P. J., Tobo, Y., Hartmann, S., Raddatz, M., Clauss, T., Niedermeier, D.,
862 and Stratmann, F.: Kaolinite particles as ice nuclei: learning from the use of different types of
863 kaolinite and different coatings. *Atmos. Chem. Phys.*, 14, 5529–5546, 2014.

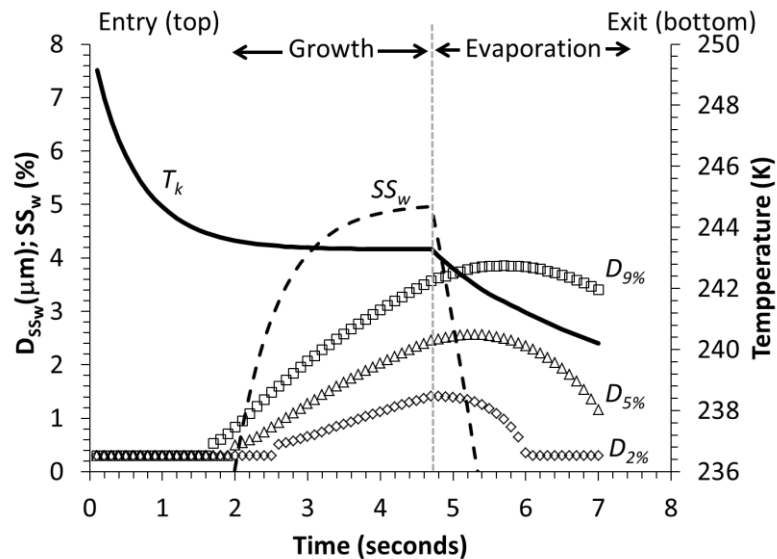
864 Wright, T. P., and Petters, M. D.: The role of time in heterogeneous freezing nucleation, *J.*
865 *Geophys. Res. – Atmos.*, 118, 3731–3743, doi:10.1002/jgrd.50365, 2013

866

867 Table 1. Equivalent experiment comparisons between CFDC and AIDA

Project	Expt	INP type	T (K)	AIDA-INP fraction	CFDC-INP fraction	$n_{a>0.5\mu\text{m}}$ (cm^{-3})	S_{tot} ($\mu\text{m}^2 \text{cm}^{-3}$)
ICIS	23	CID	247.9	0.0009	0.0012	36.0	61
ICIS	20	SD	249.7	0.0023	0.0038	28.0	102
ACI03	43	Amb	238.3	0.0009	0.0002	10.1	246
ACI03	9	AD2cSOA	245.1	0.0032	0.0018	58.0	226
ACI03	7	AD2cSOA	245.6	0.0080	0.0025	29.0	117
ACI03	2	AD2	248.2	0.0008	0.0010	0.8	2.3
ACI03	3	AD2	247.2	0.0005	0.0005	0.6	3.1
ICIS	26	Snomax	265.2	0.0052	0.0060	88.0	1089

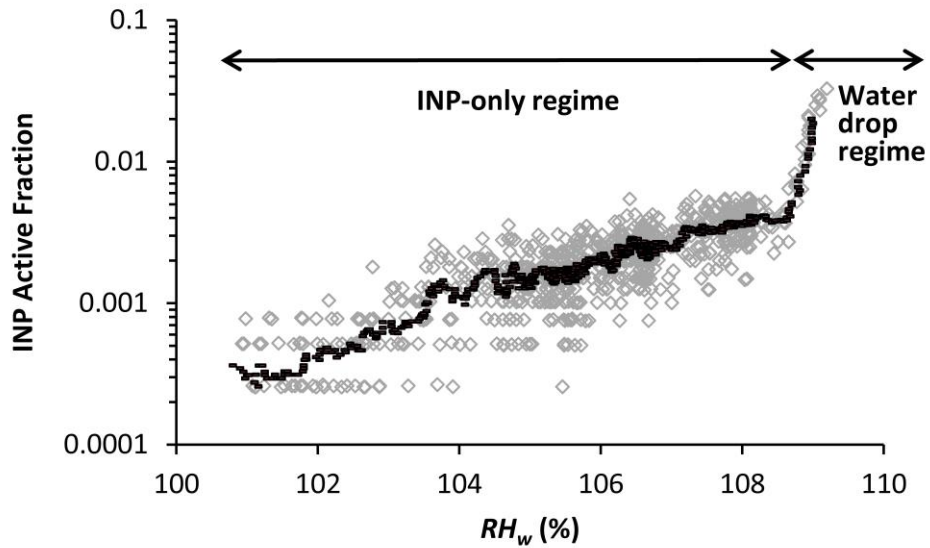
868



869

870 Figure 1. Calculated time-dependent temperature in Kelvin (T_k), and supersaturation ($SS_w =$
 871 $RH_w - 100\%$) for a potential INP starting at $0.3 \mu\text{m}$ diameter and cooling to a target
 872 temperature of -30°C and steady state SS_w of $\sim 5\%$ in transit through the CFDC, using the
 873 model of Rogers (1988). Droplet diameter is shown for these calculated conditions ($D_{5\%}$) and
 874 for conditions of SS_w approaching 2% ($D_{2\%}$) and 9% ($D_{9\%}$) in the growth region prior to the
 875 point of transition into the ice saturated (evaporation) region of the CFDC. Perfect water
 876 accommodation is assumed for these growth rate calculations. Flow rates specified are
 877 equivalent to those used in data collection for most samples used in this study, with a total
 878 residence time of 7 seconds.

879



880

881 Figure 2. INP active fraction of mineral dust particles versus RH_w during a “scan” of RH_w
 882 from low to high values during CFDC sampling from the AIDA chamber prior to a “first
 883 expansion” cloud formation experiment using a Saharan Dust (type SD, AIDA Experiment
 884 #20, September 25, 2007)) aerosol distribution with $n_a = 411 \text{ cm}^{-3}$, $d_g = 0.18 \text{ }\mu\text{m}$ and $\sigma_g =$
 885 2.14. A 15 s running mean line overlays 1Hz data points. The regions of continuously
 886 increasing ice active fraction is distinguished from the region of onset of cloud droplet
 887 contamination of the ice signal above 108.5% RH_w . Aerosol lamina temperature was
 888 maintained at 249.7 K during the scan.

889

890

891

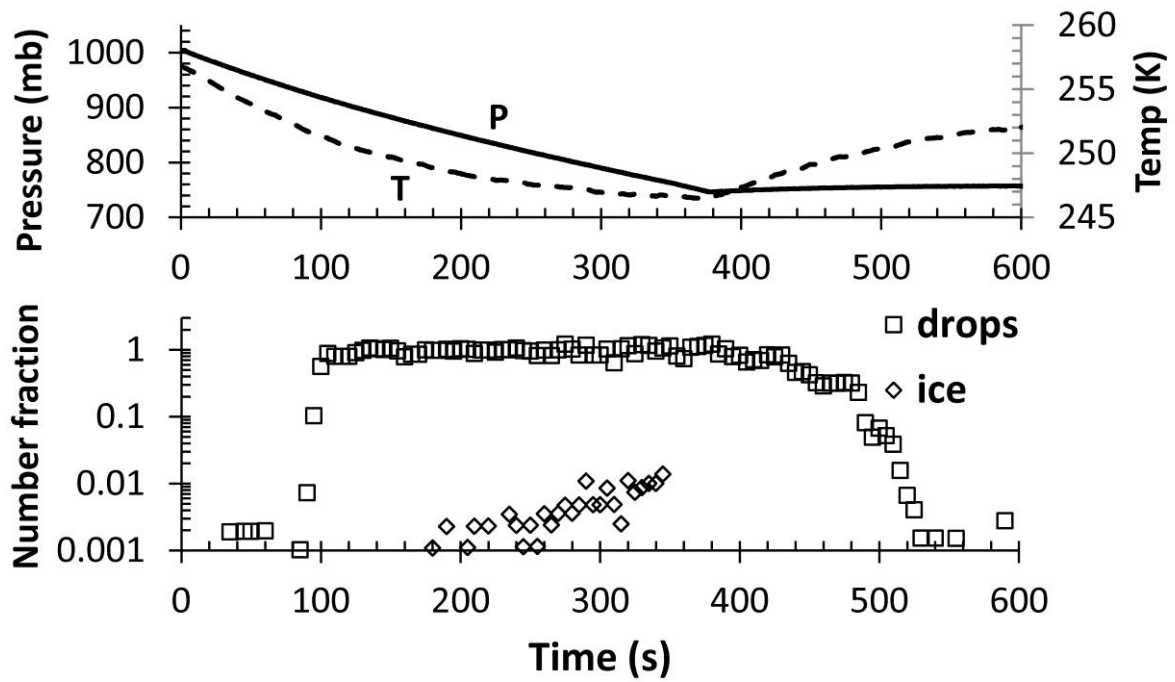
892

893

894

895

896



897

898 Figure 3. Temperature, pressure, and the number fractions of particles in droplets and ice
 899 crystals for the ICIS 2007 AIDA cloud expansion experiment #22 using Saharan dust
 900 aerosols. The data (0.2 Hz as plotted) indicate the complete activation of particles to cloud
 901 droplets and minor fractions of these particles activating as INPs as the chamber temperature
 902 cools. Calculation of ice-active fraction is suspended at the point of strong ice crystal
 903 sedimentation after 350 s.

904

905

906

907

908

909

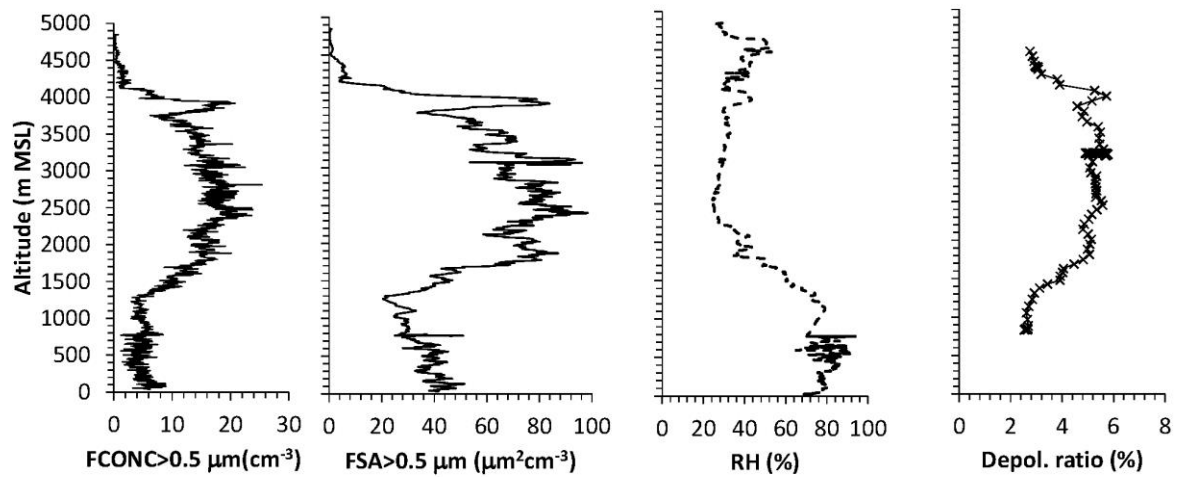
910

911

912

913

914

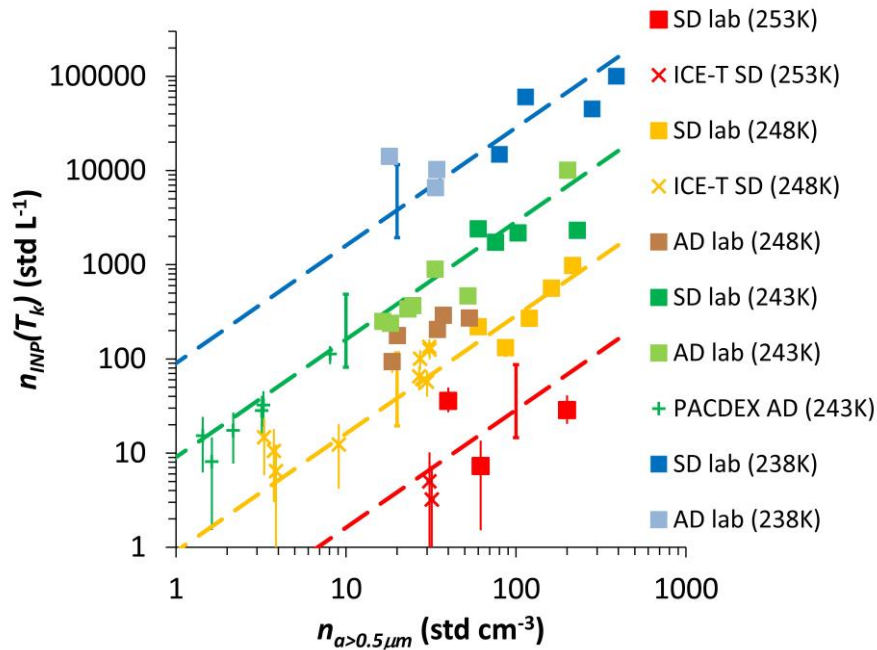


915

916 Figure 4. Vertical profiles during descent sounding by C130 aircraft on July 4, 2011 during
917 the ICE-T study. Panels from left to right, respectively, are FSSP-300 ambient particle
918 concentrations in clear air at optical diameters larger than 0.5 μm, FSSP-300 surface area in
919 the same size range, relative humidity and lidar linear depolarization ratio.

920

921



922

923 Figure 5. Relations between CFDC INP number concentrations measured at a nominal value
 924 of 105% RH_w and $n_{a>0.5 \mu m}$ in laboratory (lab) and field (PACDEX and ICE-T) measurements
 925 of Asian (AD) and Saharan (SD) dust particles at temperatures of approximately 253, 248,
 926 243 and 238 degrees Kelvin. Dashed lines are not best fits for each temperature, but are
 927 instead determined from the empirical fit given by Eq. (2) ($cf = 1$, $\alpha = 0$, $\beta = 1.25$, $\gamma = 0.46$,
 928 and $\delta = -11.6$). Uncertainties in observational data, given as twice the Poisson sampling error
 929 for the time-integrated samples, are shown by vertical error bars on data points. Note that at
 930 higher n_{INP} these error bars are not visible beyond the plotted point size. Representative
 931 measures of standard error in the predicted lines (see Fig. 6) are shown by capped error bars.

932

933

934

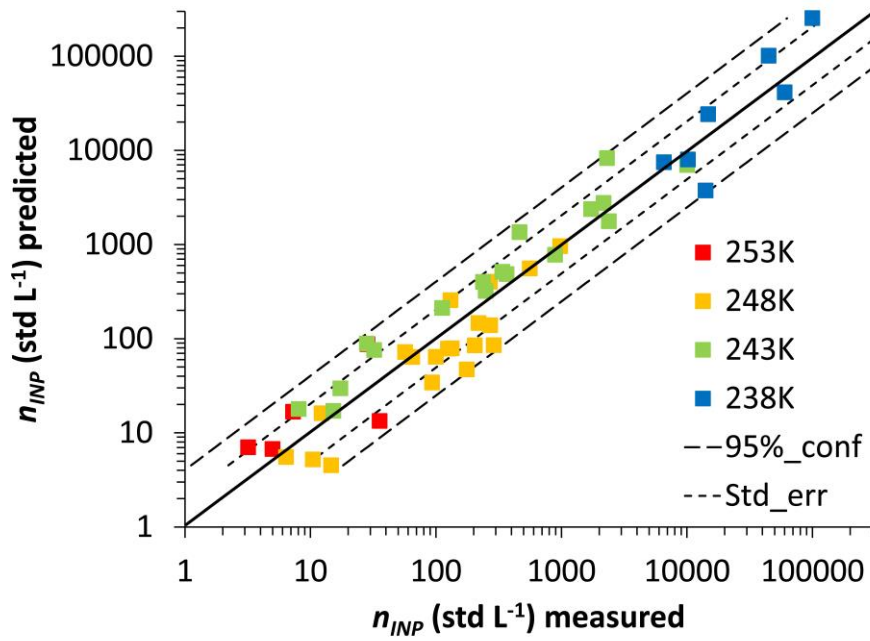
935

936

937

938

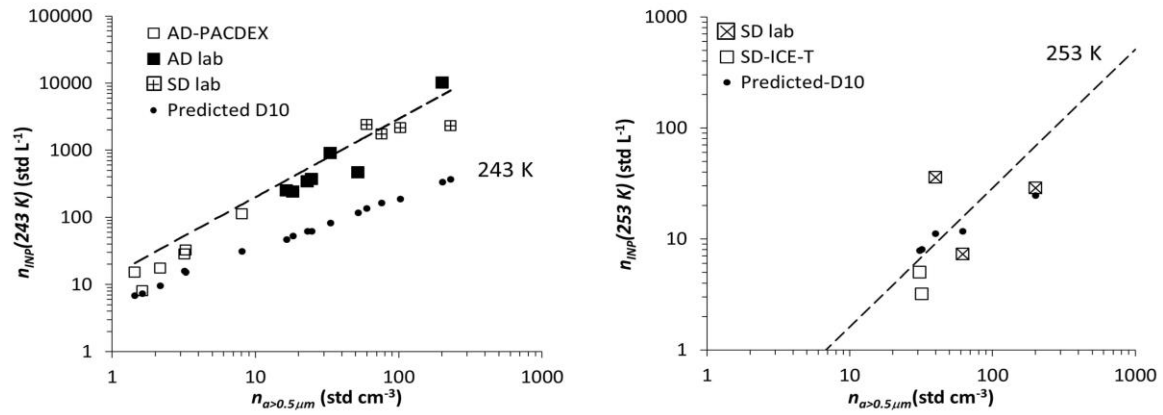
939



940

941 Figure 6. Prediction of Eq. 2 ($cf = 1$, $\alpha = 0$, $\beta = 1.25$, $\gamma = 0.46$, and $\delta = -11.6$), plotted versus
 942 raw field and laboratory data collected at 105% RH_w (Fig. 5), with lines added around the 1:1
 943 line (solid) to indicate standard error (short-dashed) and 95% confidence intervals (long-
 944 dashed).

945



946

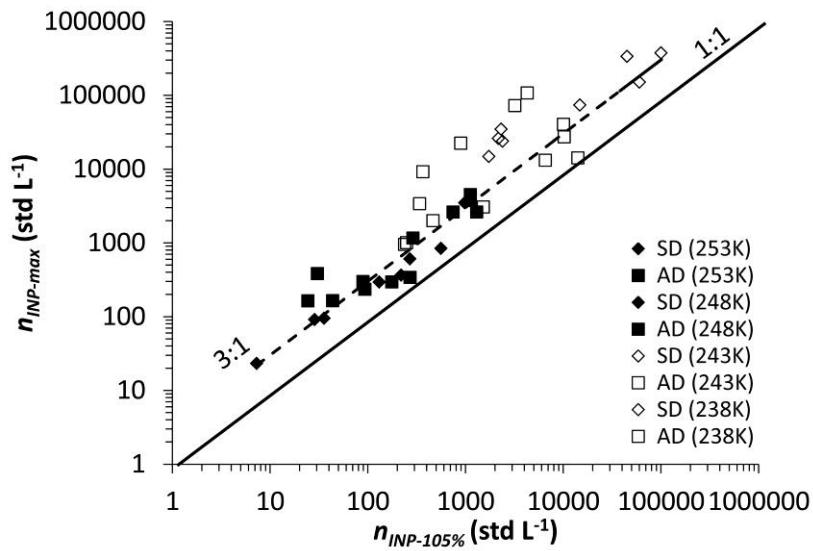
947 Figure 7. As in Fig. 5, but comparing raw (Fig. 5) and predicted ($cf = 1$) results to the D10

948 parameterization (calculated for the same data) at nominal temperatures of 243 K and 253 K.

949 Note that the D10 parameterization does not produce a straight line in the panel figures due to

950 the variation of temperature within 1 K that was allowed in the analysis.

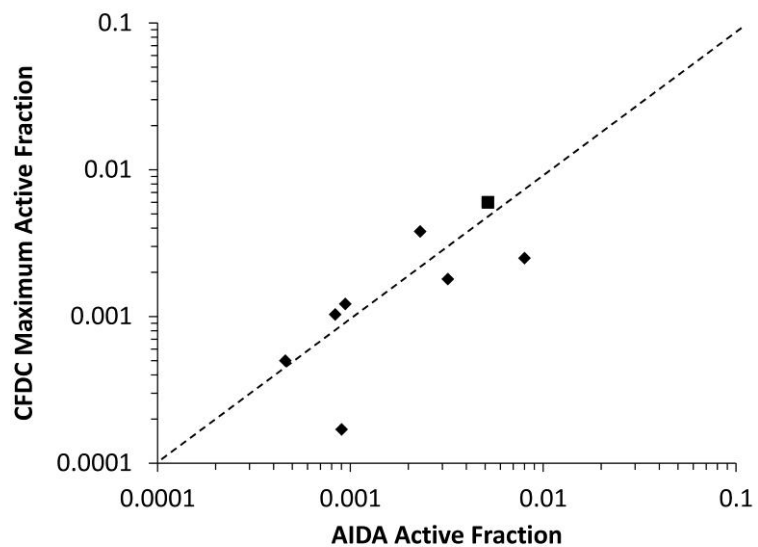
951



952

953 Figure 8. CFDC INP number concentration at peak RH_w values (preceding droplet
 954 breakthrough) in comparison to n_{INP} measured at 105% RH_w . A range of temperatures from
 955 approximately 253 to 238 K are represented, as shown. The dashed line expresses $cf = 3$ as a
 956 uniform correction on INP number concentration for this selection of data.

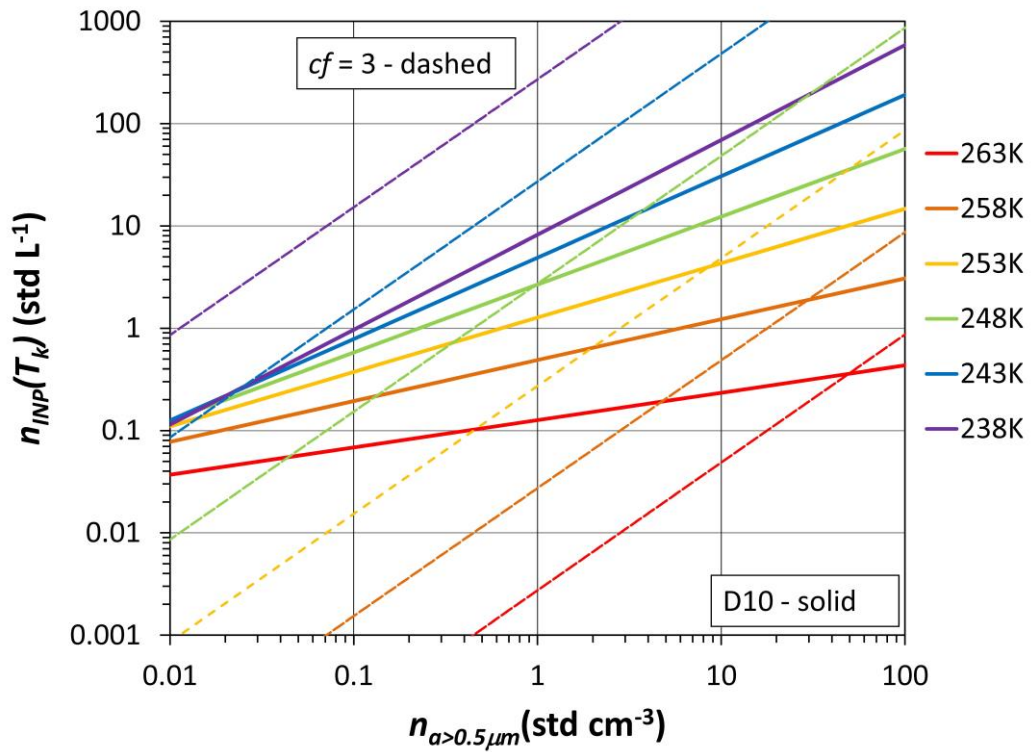
957



958

959 Figure 9. Comparison of CFDC maximum INP active fraction and AIDA cloud expansions
 960 active fractions for common experiments when the CFDC sampled from the AIDA chamber
 961 prior to first expansion. The square point is for an experiment using SnomaxTM particles.

962



963

964 Figure 10. Comparison of ice nucleation parameterization from this study (Eq. 2 with $cf = 3$),
 965 with the D10 parameterization for calculations in the mixed-phase cloud regime.

966

967

968

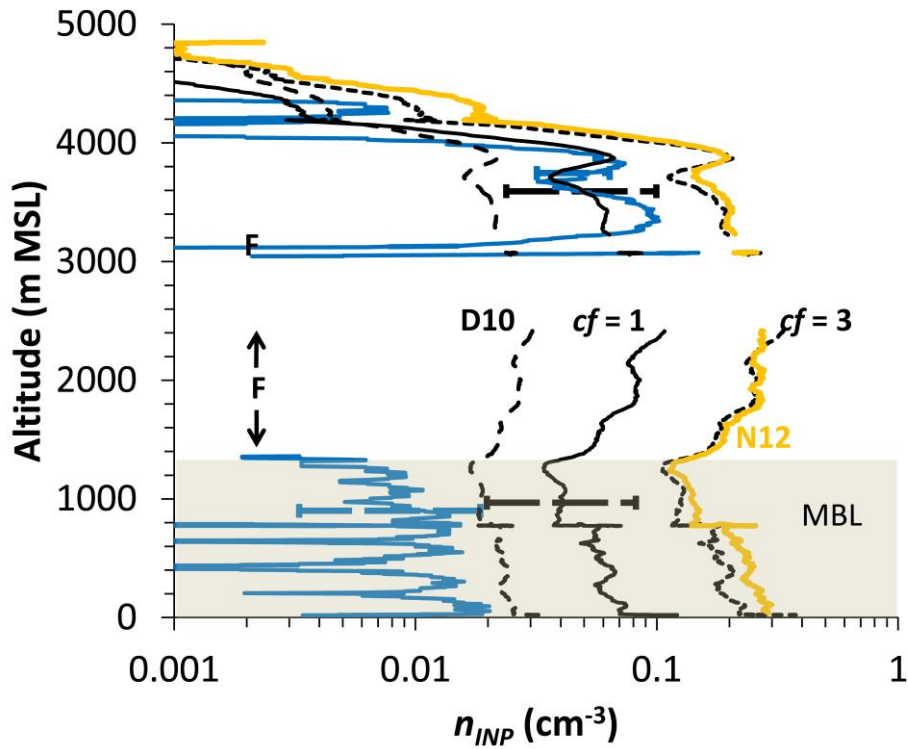
969

970

971

972

973

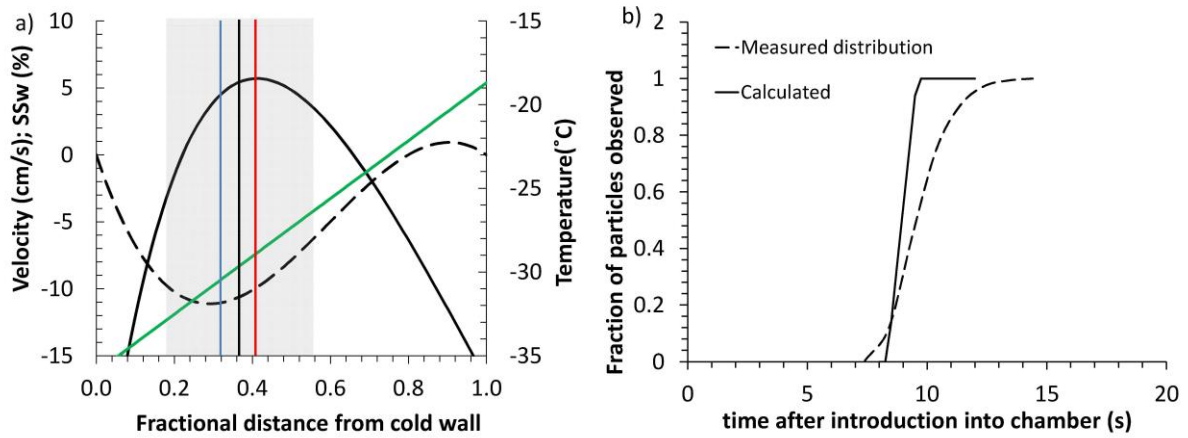


974

975 Figure 11. Comparison of ice nucleation data and parameterizations for data collected
 976 onboard the NSF/NCAR C-130 aircraft during the ICE-T study descent sounding through a
 977 Saharan dust layer shown in Fig. 4. CFDC INP data plotted as a 30-s running average at
 978 ambient conditions are given by the blue trace, the D10 parameterization is the long-dash
 979 trace, the solid black trace labeled $cf = 1$ is the uncalibrated parameterization derived using
 980 Eq. 2 ($\alpha = 0$, $\beta = 1.25$, $\gamma = 0.46$, and $\delta = -11.6$), and the short-dash trace labeled $cf = 3$ is the
 981 calibration-corrected parameterization with the same coefficients, both also corrected from
 982 STP to ambient INP concentrations. Uncertainties representing twice the Poisson sampling
 983 error of the 30-s running average data are given at two altitudes, and the standard errors of
 984 the $cf = 3$ prediction are shown at two nearby altitudes. Plotted for comparison is the
 985 parameterization of Niemand et al. (2012), using aerosol surface area and CFDC processing
 986 temperature as input. CFDC processing temperature cooled from 248 K at 5 km to 246 K at
 987 landing, while CFDC calculated RH_w at the lamina position was maintained at $105 \pm 0.5\%$.
 988 The shaded region represents the marine boundary layer (MBL). Label F indicates that CFDC
 989 sample air was being filtered. The data gap is when CFDC flow was shut off to remove an ice
 990 crystal impactor.

991

992



993

994 Figure B1. a) A schematic depiction of a particle beam (shading) spread to a breadth of 4
 995 times the ideal positions of the cold (blue) and warm (red) edges of the aerosol lamina on the
 996 basis of transit time measurements of a 1 s wide aerosol pulse through the CFDC column (b).
 997 The transit time measurement for a lamina central temperature of -30°C and $105\% \text{RH}_w$ is
 998 compared to that calculated for a uniform distribution of particles residing fully within the
 999 aerosol lamina. Other calculated values in a) are the temperature profile (green), SSw (solid
 1000 black), and downward (negative) air velocity (dashed) in the gap between the CFDC walls.

1001

1002

1003

1004

1005

1006

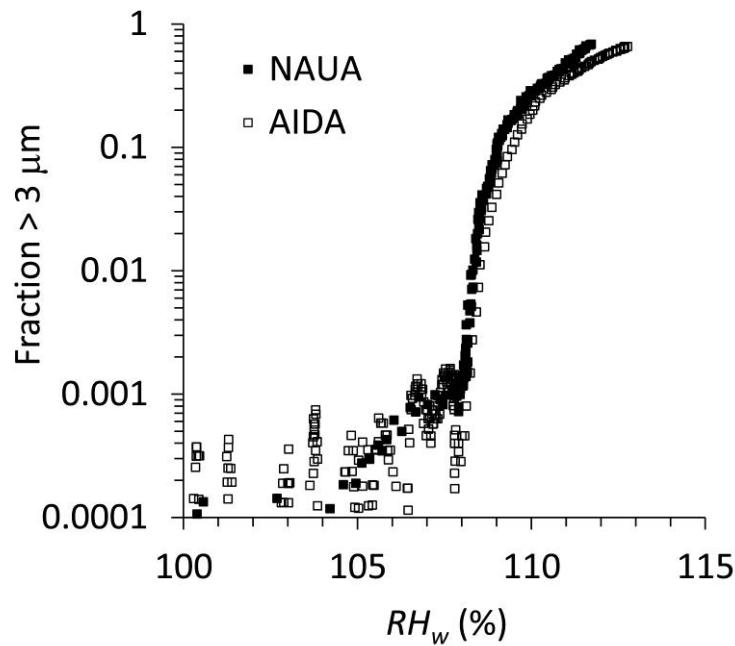
1007

1008

1009

1010

1011



1012

1013 Figure B2. As in Fig. 2, raw 1 Hz CFDC data from an ICIS-2007 experiment on September
 1014 24, 2007 showing the fraction of total aerosol concentrations (measured by a CPC) appearing
 1015 at OPC sizes above 3 μm during RH_w scanning for two experiments at -21°C when processing
 1016 particles from a dust sample that had been collected following a dust storm in Israel (Kanji et
 1017 al., 2011). The data termed NAUA was sampled following dispersion into a 4 m^3 aerosol
 1018 chamber, with concentrations of approximately 5000 cm^{-3} present at the time of sampling.
 1019 The data termed AIDA was sampled directly from the AIDA expansion chamber prior to a
 1020 cloud expansion, when the total particle concentrations were approximately 100 cm^{-3} . Water
 1021 droplet breakthrough of the CFDC evaporation region occurs at $\sim 108\%$ in each case and
 1022 progressively more activated cloud droplets survive through the evaporation region as RH_w is
 1023 increased further.